DVB-T Receiver Independent of Channel Allocation, With Frequency Offset Compensation for Improving Resolution in Low Cost Passive Radar

Pedro-José Gómez-del-Hoyo, María-Pilar Jarabo-Amores, *Member, IEEE*, David Mata-Moya, *Member, IEEE*, Nerea del-Rey-Maestre, *Member, IEEE*, and Manuel Rosa-Zurera, *Senior Member, IEEE*

***Abstract*—In this article, a commercial low cost solution for increasing DVB-T based passive radar (also referred to as passive coherent location) robustness with respect to channel allocation and range resolution, is designed. IDEPAR demonstrator is updated to include a new recording system in charge of DVB-T channels reallocation. The use of commercial hardware introduces frequency mismatching between acquired channels that compromises system operation. To face channel frequency alignment, fulfilling the requirements imposed by the high Doppler resolution typical of passive radars, a novel compensation algorithm is proposed, based on the minimization of signal dispersion in the Cross-Ambiguity Function domain. The well-known cyclic prefix van de Beek method is used as reference. Results show an increase in target signal to interference ratio and detection performances, as well as a reduction of clutter dispersion when the novel proposed algorithm is applied. The low cost solution is also compared to a high performance one capable of acquiring a wide bandwidth of sparse DVB-T channels, and performing channel reallocation by digital signal processing. Results show that both systems reached similar performances in terms of range resolution and SNR improvement.**

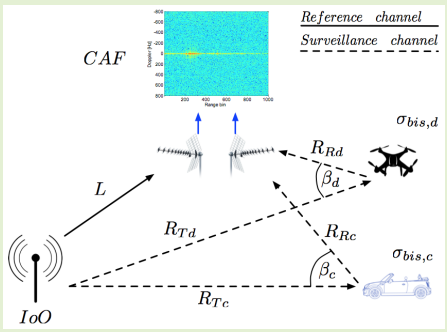

***Index Terms*— Passive radar, passive coherent location, multistatic radar, DVB-T, COTS components, channel allocation, frequency alignment, wideband.**

I. Introduction

PASSIVE Radars (PRs), also referred to as passive coherent location, are promising candidates to complement/substitute active ones in security and defence applications. PRs are defined as a set of techniques to detect targets and to estimate parameters using non-cooperative signals (such as broadcast, communications, radar, or radio-navigation signals) as Illuminators of Opportunity (IoOs) [1]. As a result, PR are a class of multistatic radar. They overcome all active radar drawbacks associated to the use of a dedicated transmitter. On the other hand, Commercial Off-The-Shelf (COTS) devices can be used for signal reception (antenna, RF front-end and acquisition systems). The lack of control over the IoO imposes the use of two-channel reception systems in the bistatic configuration considered in this article (the reference one, to acquire the direct signal from the IoO, and the surveillance one to capture targets' echoes), and complex detection and tracking techniques. An intensive research has been carried out in the last two decades on PRs [2]–[5].

The first PRs used analogue signals, such as analogue television and FM broadcasting [6]–[8], but they have low and data dependent bandwidths. In contrast, digital signals provide higher and data-independent bandwidths: Digital Audio Broadcast (DAB) and Digital Radio Mondiale (DRM) [9],

Manuscript received June 5, 2020; revised July 12, 2020; accepted July 15, 2020. Date of publication July 22, 2020; date of current version November 18, 2020. This work was supported in part by the Spanish Ministry of Science, Innovation and Universities under Grant RTI2018-101979-B-I00 and in part by the Junta de Castilla la Mancha FEDER under Grant SBPLY/19/180501/000350. The associate editor coordinating the review of this article and approving it for publication was Dr. Marco J. Da Silva. *(Corresponding author: Pedro-José Gómez-del-Hoyo.)*

The authors are with the Signal Theory and Communications Department, University of Alcalá, 28805 Alcalá de Henares, Spain (e-mail: pedrojose.gomez@uah.es; mpilar.jarabo@uah.es; david.mata@uah.es; nerea.rey@uah.es; manuel.rosa@uah.es).

Digital Object Identifier 10.1109/JSEN.2020.3011129

TABLE I
DVB-T PHYSICAL CHANNEL DISTRIBUTION IN THREE SPANISH PROVINCES: MADRID (MAD.), BARCELONA (BAR.) AND VALENCIA (VAL.)

Physical channel	Mad.	Bar.	Val.	Physical channel	Mad.	Bar.	Val.
22	*X*		*X*	**43**			*X*
23		*X*	*X*	**44**		*X*	
26	*X*	*X*		**46**			*X*
27		*X*		**47**	*X*		
28			*X*	**48**		*X*	
29		*X*		**49**	*X*		
31		*X*		**50**	*X*		
33	*X*	*X*		**55**	*X*		
34		*X*		**57**			*X*
39	*X*			**58**	*X*		*X*
40		*X*	*X*	**59**	*X*		
41	*X*	*X*					

Global System for Mobile (GSM) [10], Universal Mobile Telecommunication System (UMTS) [11], Digital Video Broadcasting-Terrestrial (DVB-T) [12], [13].

DVB-T based PRs are under intensive research due to their transmitted power, high availability, known position and waveform, good autocorrelation characteristics, channel bandwidth ($\simeq$ 8 MHz), and the possibility of using consecutive channels for increasing PR range resolution [14]–[16]. This is a key feature for the development of passive radar imaging techniques [17]–[20].

Each DVB-T physical channel is associated to a stream of digital data carrying one or more services that is denoted as Multiplex (MX). In Spain, multichannel PRs could exploit the three consecutive higher MXs centred on 850MHz, that concentrated most of DVB-T emissions before the analogue switch-off. It gave rise to a reallocation of the higher frequencies DVB-T MXs to allow LTE 800MHz band transmissions. The new DVB-T MXs allocation is characterized by high spatial variability (in a same country, it can vary significantly from one region to another), and frequency sparsity, reducing the probability of finding consecutive MXs (Table I). Nowadays, a second reallocation is in progress, that will release the frequency band ranging from 694 MHz to 790 MHz, for new 5G communication services.

In [21]–[24] a solution for exploiting multiple non-consecutive channels from a single IoO was presented. A new reception stage called *recording equipment* was included between the Radio-Frequency chain and the acquisition one, to shift the selected non-consecutive channels, and build a new spectrum composed of consecutive shifted channels with a predefined guard band. These previous works presented a rigorous mathematical model and proposed solutions to important problems that impact PR performance:

- Due to the use of different MXs with different carrier frequencies, target echoes are the result of the combination of different Doppler components, one per carrier frequency. A frequency correction term was proposed for correcting this effect, an extension of that proposed in [25].
- Although an ideal recording system was assumed, a phase correction was required to achieve the integration gain improvement associated to the higher processing bandwidth [26].
- The different channels were not phase synchronized due to different factors: although a unique IoO was considered, each carrier suffered different propagation phase delays; Doppler shifts associated to moving targets depended on the carrier frequency; the reflection gain of desired targets and clutter sources were modelled as stochastic processes.

The proposed solutions were evaluated on synthetic data, without considering the implementation of the recording equipment and potential associated errors. Another important characteristic is that proposed frequency and phase corrections were calculated for each target, using target parameters provided by previous detection and tracking stages exploiting a single MX (with the resolution and integration gain associated to a single MX) [26].

In the current paper, the implementation of such recording equipment is tackled, defining design requirements and processing architectures that guarantee low development and maintenance costs, which are distinctive features of PRs. These are more important in PRs using surveillance array antennas and digital array signal processing techniques, which are key approaches to improve PR performance with respect to angular coverage and resolution, 3D (range, Doppler and azimuth) detection and tracking, and radar imaging [27]–[29]. In these solutions, a recording equipment per single radiating element of the antenna array would be necessary, in addition to that required for the reference channel.

Ideally, configurable high quality frequency conversion stages are the main components of each recording equipment, in order to allow the shift of the selected channels to build a new spectrum compatible with the central frequency and bandwidth defined by the acquisition stage. On the other hand, channel allocation can be quite different from one emplacement to another, in different regions of a country or in different countries, therefore the recording equipment is required to allow the selection and shift of any set of DVB-T MXs along the complete DVB-T frequency band. These are high quality requirements, which are provided by high cost devices. In this article, an alternative low cost solution is designed based on commercial frequency converters used for DVB-T home distribution. These devices are analysed to identify sources of distortion in the PR operation due to the use of a non-ideal recording equipment. Design requirements are defined and improved signal processing techniques are proposed for distortion compensation:

- A new frequency alignment method is proposed to reduce residual errors at the frequency alignment stage. The van de Beek algorithm [30], which was designed for direct reception of Orthogonal Frequency Division Multiplexing (OFDM) signals, is used as reference solution.
- A frequency correction algorithm is proposed for correcting the target Doppler spreading effect due to the use of different carrier frequencies. The solution proposed in [26] must be applied to each previously detected target, whereas the proposed one works on regions of the Cross Ambiguity Function (CAF). As a result, the detector can be designed considering the signals made up of multiples MXs.

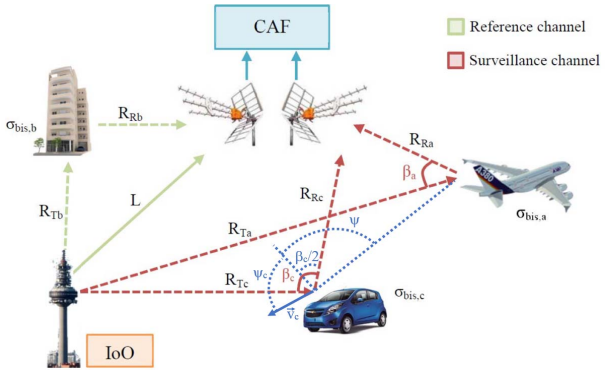

Fig. 1. Basic geometry of a bistatic PR: R_{Ti}, R_{Ri} and L are the target-to-transmitter, target-to-receiver, and transmitter-to-receiver distances, respectively; β_i is the bistatic angle, ψ_c and ψ are the angles defined by the car bistatic bisector, $\beta_c/2$, and the car speed vector, $\bar{v}_c$, and the line joining both targets, respectively. $\sigma_{bis,i}$ is the tragets' bistatic radar cross section ($i \in \{b,c,a\}$ refers to *building*, *car*, and *airplane*, respectively).

IDEPAR (Improved DEtection techniques for PAssive Radars), the PR demonstrator developed by the University of Alcalá [16], was used to validate the proposed recording equipment and the distortion compensation techniques. A reference processing architecture was also implemented, based on high performance acquisition boards capable of acquiring 80MHz of instantaneous bandwidth in the DVB-T frequency band. Digital processing techniques were applied to select and shift in frequency a set of MXs. A comparative study was carried out to distinguish the effect of carrier and targets Doppler phase delays associated to signal features and propagation effects, and residual errors generated by non-ideal receiver components in the proposed low cost solution. The main objective of this article is to prove the suitability of the proposed low cost approach, based on commercial systems for DVB-T home distribution and new algorithms for reducing their non-ideal effects; the reduction of residual frequency and phase unbalance due to signal features and propagation effects, will be tackled in future works.

The rest of the paper is structured as follows: Section II summarizes the principle of operation of PRs. Recording system requirements and the hardware solution are presented in Section III. The compensation method proposed in [30] is analysed in Section IV; a novel compensation algorithm is described in Section V. Both methods are compared using real data in Section VI. Finally, conclusions are presented in Section VII.

II. Passive Radar Operating Principle

The basic geometry of a bistatic PR is depicted in Figure 1. It is composed of a reference channel that acquires the direct signal from the IoO and a surveillance one in charge of acquiring the targets' echoes. Both acquired channels are coherently processed by the Cross Ambiguity Function (CAF) [31]. The bistatic radar cross section, $\sigma_{bis,i}$, models the energy scattered by the desired targets and clutter sources towards the PR when they are illuminated by the IoO.

The CAF is the core of the coherent processing. It performs the matched filtering, allows the estimation of the bistatic range and Doppler shift of the target, and provides the necessary signal processing gain. To generate the CAF, delayed and Doppler-shifted copies of the reference signal, $s_r[n]$, are correlated with the surveillance one, $s_s[n]$ (1) [6], [7]. This requires a coherent acquisition of both channels preserving their phase information.

$$S^{CAF}[m,p] = \sum_{n=0}^{N-1} s_r^*[n-m] \cdot s_s[n] \cdot \exp^{-j2\pi \frac{p}{N} n} \quad (1)$$

$N = T_{int} \cdot f_s$, is the number of samples, being T_{int} (s) the integration time, which defines the duration of the Coherent Processing Interval (CPI), and f_s (Hz) the sampling frequency; m is the time bin associated with a delay $\tau_m = m/f_s$, and p is the Doppler-shift corresponding to $f_{dop} = f_s \cdot p/N$. For each scatterer, the result of the CAF is the Ambiguity Function (AF) of the transmitted signal, scaled and shifted to be centred on the scatterer bistatic time delay and Doppler shift. The bistatic time delay is calculated as $(R_T + R_R)/c - (L/c)$, being c the light speed.

If the PR receiver and the IoO are stationary, a target, T_1, with speed vector $\mathbf{v}_1 = V_1\tilde{v}_1$, present a bistatic Doppler shift $f_{D1}(Hz) = (2 \cdot V_1/\lambda) \cdot \cos(\psi_1) \cdot \cos(\beta/2)$ (ψ_1 is defined by the target speed vector and the bistatic bisector) [31]. Stationary targets' CAF peaks appear along the zero Doppler line of the CAF output domain (Range-Doppler Map, RDM), although their contributions spread throughout all the RDM.

This processing scheme requires a complete coherence among all the receiving channels: one reference and one surveillance channel if a single surveillance antenna is used; multiple channels if digital array signal processing techniques are applied, one for each single radiating element. All the Local Oscillators (LOs) of the intermediate frequency conversion stages must be locked, and the ADCs must be synchronized in frequency and phase.

A delay difference between two targets echoes equal to or greater than $c/2B$, being B the signal bandwidth, allows targets separation. In bistatic systems, the associated range resolution is calculated as $\Delta_{R_b} = c \cdot cos(\beta/2)/(2 \cdot B \cdot cos(\psi))$, being ψ the angle defined by the line connecting both targets and the bistatic bisector associated to one of them [31]. On the other hand, Doppler resolution is determined by T_{int}, $\Delta_{f_{Doppler}} = 1/T_{int}$. As the CAF integration gain is equal to $T_{int} \cdot B$, PRs use long T_{int} values, giving rise to high Doppler resolutions, usually of the order of Hz.

The DVB-T MX spectrum depends on several parameters that are selected by each country. In Spain, each DVB-T MX is composed of a centred data bandwidth of 7.607157 MHz and two adjacent guard bands to complete an 8 MHz bandwidth [32]. Therefore, for a DVB-T MX, $B_1 \simeq 7.6MHz$, $\Delta_{R_b} \simeq 19.74 \cdot cos(\beta/2)/cos(\psi)$ (m). In [14]–[16], the use of $N = 3$ consecutive DVB-T MXs increased Δ_{R_b} by a factor of 3. But if consecutive channels are not available, an acquisition bandwidth $B = N \cdot B_1$, with $M < N$ DVB-T channels, will provide a range resolution increasing factor of M, instead of N [33]. In [21]–[24], a deep study of multichannel signal processing is carried out. Instead of designing an acquisition chain with an instantaneous bandwidth equal to $N \cdot B_1$,

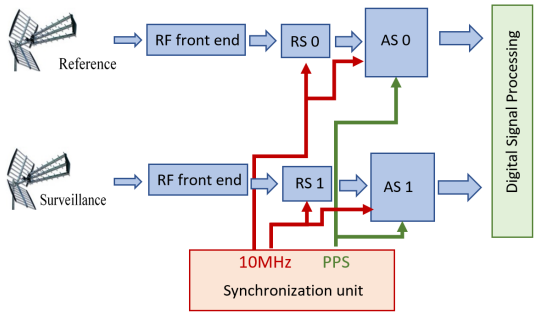

Fig. 2. Architecture of a PR receiver with a single surveillance antenna, including the recording systems (RS0 and RS1) before the acquisition systems (AS0 and AS1) in both reference and surveillance channels.

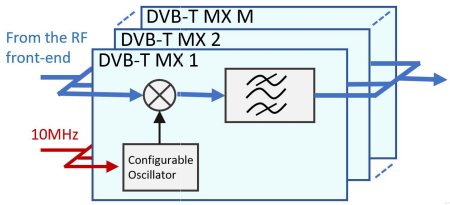

Fig. 3. Functional block of a recording system capable of performing the independent frequency conversion of M DVB-T MXs.

composed of $M < N$ non-consecutive channels, the available channels are shifted to generate a set of M consecutive ones, reducing the instantaneous bandwidth of the acquisition chain to $B = M \cdot B_1$. Carrier delays and targets' Doppler shifts will be different for the different carrier frequencies, that, in contrast with the study cases considered in [14]–[16], [33] can be significantly separated, and frequency and phase compensation techniques are required for achieving theoretical integration gain and range resolution values. In the current paper, this approach is considered, and the effects of non-ideal recording system components are included in the received signal model, with a first objective of compensating them, generating a compensated signal suitable for the application of frequency and phase corrections proposed in [21]–[24].

III. Recording System Requirements and Hardware Solution

Figure 2 shows the architecture of the PR receiver based on the recording system approach for the simplest case, using a single surveillance antenna. This architecture can be extended to antenna arrays. Each reception chain is composed of a RF front end, whose main elements are filters and Low Noise Amplifiers (LNAs); the Recording System (RS$i, i = 0, 1$), and the Acquisition System (AS$i, i = 0, 1$), which includes the frequency down conversion and digitalisation stages. A synchronization unit provides a reference 10MHz clock to RSs and ASs modules, to lock the frequency converters' LOs and the sampling frequencies, respectively; and a Pulse Per Second (PPS) signal to the ASs for sampling phase synchronization.

The functional block of a RS is presented in Figure 3. It is composed of M sub-modules to receive a set of M DVB-T MXs, and generates a continuous output spectrum resulting from shifting the acquired MXs in the frequency domain. To guarantee PR robustness with respect to DVB-T MXs availability, the set of M DVB-T MXs to be acquired should be configurable; to allow the integration of the RSs in any operating PR, the central frequency of the output signal should be also configurable.

PR operation is based on the coherent processing of the reference and surveillance channels, which requires high quality configurable-LOs and frequency converters in each RS submodule. Frequency drifts and phase noises of the LOs of the different sub-modules will distort the acquired signals, giving rise to PR performance losses that can be critical. Commercial devices fulfilling these quality requirements are characterized by high costs. Considering the proposed functional block (Figure 3) and the extended use of surveillance array antennas in PRs for digital array signal processing, the cost of the global system can be dramatically increased.

A. Commercial Multichannel SDR Solutions. The IDEPAR Demonstrator

There are different low cost multichannel SDR solutions in the market that can synchronously digitalise sparse channels in a high frequency band. The hardware architecture described in [34] provides high versatility and easy scalability. Acquisition bandwidths are usually limited to several MHz, which are suitable for PRs based on FM or DAB IoOs. In multichannel DVB-T based PRs, multiple SDRs devices can be combined for acquiring the desired bandwidth, which should be a multiple of the MX one. As a result, the overall system complexity increases (use of multiple splitters that decrease the signal level available for the SDRs; number of required communication interfaces…). Furthermore, typical integrated ADCs have 8 resolution bits, reaching an ideal quantification SNR of 49dB, which can limit the dynamic range. Noise level is mainly determined by the first element of the RF front end, that is usually a Low Noise Amplifier (LNA), whereas the maximum signal at the input of the surveillance antenna depends on the available IoO (trasmitted power and distances to the PR and to the area of interest, that will define DPI and the strongest clutter return levels). Taking into consideration that typical commercial LNAs provide a noise factor of 0.8dB, in the case study presented in section VI.VI-A the maximum expected SNR is around 70dB (higher than the 49 dB calculated for the ideal 8 bits ADC).

Other medium cost solutions with higher acquisition performances are available in the market [35]. The USRP B200 by Ettus provides a maximum sampling rate of 61.44 MS/s with an ADC resolution of 12 bits. However, the USB 3.0 communication interface performance varies dramatically when multiple devices are streaming through the same controller, limiting the number of acquisition channels and effective acquisition bandwidth.

IDEPAR is based on USRP N210 devices [36], that mount a 14 bits ADC, and provide a maximum instantaneous bandwidth of 25 MHz limited by the 1Gb Ethernet interface [16]. The maximum SNR, assuming and ideal ADC, is 86.04dB. The detection performance of this architecture depends on the

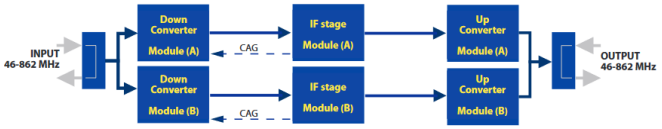

Fig. 4. Televes Twin A/D T.0x block diagram [38]. Frequency conversion scheme implemented by the commercial solution.

number of available consecutive MXs in the selected scenario, which probability can be really low (Table I). The proposed low cost solution for the recording system will increase IDEPAR robustness with respect to the available consecutive MXs, guaranteeing a 25MHz instantaneous acquisition bandwidth provided that there are 3 available MXs, whatever their frequency allocation is. This bandwidth will be generated after shifting the available 3 MXs in a continuous frequency range.

IDEPAR was recently upgraded adding new acquisition chains based on USRPs X310 [37], increasing the maximum instantaneous bandwidth to 100MHz, and using 10Gb Ethernet interfaces. To perform quantitative comparisons, a high performance reference processing architecture was implemented based on the USRPs X310. This system can acquire 100 MHz of instantaneous bandwidth, and digital signal processing techniques can be applied to select 3 MXs among those acquired in the 80MHz bandwidth, and shift them in frequency to generate a continuous 25MHz bandwidth. This architecture guarantees the coherent acquisition of reference and surveillance signals and, because of that, is considered as a reference in this article.

B. Proposed Low Cost Commercial Solution

The commercial solutions selected to implement the RS are the Twin A/D T.0X processors from Televes, which are widely used for DVB-T signal distribution in the home [38]. Each Twin A/D T.0X includes two conversion modules (Figure 4), so two DVB-T MX can be processed simultaneously; each module implements a two steps frequency conversion using no locked local oscillators: the first one shifts the selected MX to the passband of a high quality IF bandpass filter, and the second one performs the final conversion to the desired output frequency. The input DVB-T MX and the output central frequency can be configured. Allowed input and output frequencies are those defined by the DVB-T channel allocation, in the range from 46 to 862 MHz.

The Twin A/D T.0X processors were designed for fulfilling DVB-T signal direct reception quality requirements, whereas a PR processes the raw echo signals scattered by objects when they are illuminated by a DVB-T IoO. These echo signals are cross-correlated with the reference signal to generate the CAF. Regarding the input signal level, Twin A/D T.0X processors minimum signal level is set to -56 dBm. Reference signal level is similar to that expected in direct DVB-T signal reception, because PRs usually use a directive antenna pointing to the IoO. But the surveillance channel signal level is much lower, requiring a pre-amplification stage to fulfil sensitivity requirements. Another important issue is related to the observed output frequency drift. PRs are characterized by Doppler resolutions of the order of some Hz. Measured processor

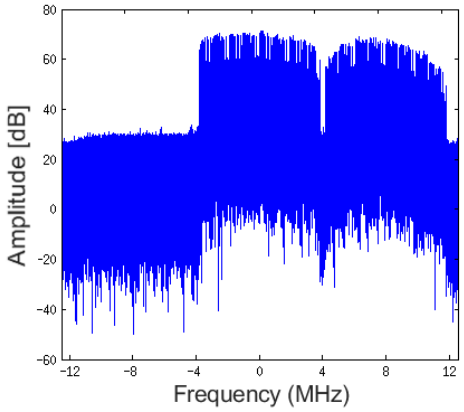

Fig. 5. Acquired signal spectrum composed of DVB-T MXs at physical channels 26 and 39 relocated in consecutive positions 43 and 44.

output frequency variations are of the order of kHz. These variations can generate artefacts in the CAF, and reduce PR detection performance. This is studied in detail in subsections III-C and III-D. The absence of local oscillators shared by the processors also results in the loss of phase lock that will affect the processing coherence. The reference and surveillance channels present a phase mismatching between acquired MXs that negatively affects the integration gain and system resolution. Target's echo phase compensation methods will be studied in future works to mitigate these pernicious effects.

C. Frequency Characterization of the Selected Solution

For the analysis of the output frequency drift of Televes processors, two modules of the same Twin A/D T.0X were configured to shift DVB-T MX at physical channels 26 (514MHz) and 39 (618MHz) to consecutive positions 43 and 44 (650 and 658MHz respectively). The Twin A/D T.0X was connected to a directional Televes antenna pointing to a DVB-T transmitter. The output two-channels signal with center frequency 654MHz and a bandwidth $B \simeq 16$MHz, was applied to the acquisition chain of the PR, which was configured for a carrier frequency equal to 650MHz. The USRP N210 converted the processor output signal to generate the in-phase and in-quadrature components, which were digitalised with a sampling frequency $f_s = 25$MHz. Figure 5 shows the acquired complex baseband signal spectrum.

Two acquisitions composed of 7 non-consecutive data blocks of 5 seconds with a temporal gap between blocks of 10 minutes were carried out. After the first acquisition, the processor was turned off during 30s, in order to evaluate the effect of restarting the modules. Spectrum analysis techniques were applied to estimate the central frequency of each data block. As the integration time for coherent processing in the PR was equal to $T_{int} = 250$ms, the central frequency was estimated for data segments of 250ms, giving rise to 20 estimated frequencies per data block.

Figure 6(a) shows the results obtained for a module of the Twin A/D T.0X, during the first acquisition of 35s. After down conversion, signal spectrum was expected to be centred at zero frequency, but the estimated frequency offset was higher than 7kHz; the differences between data blocks

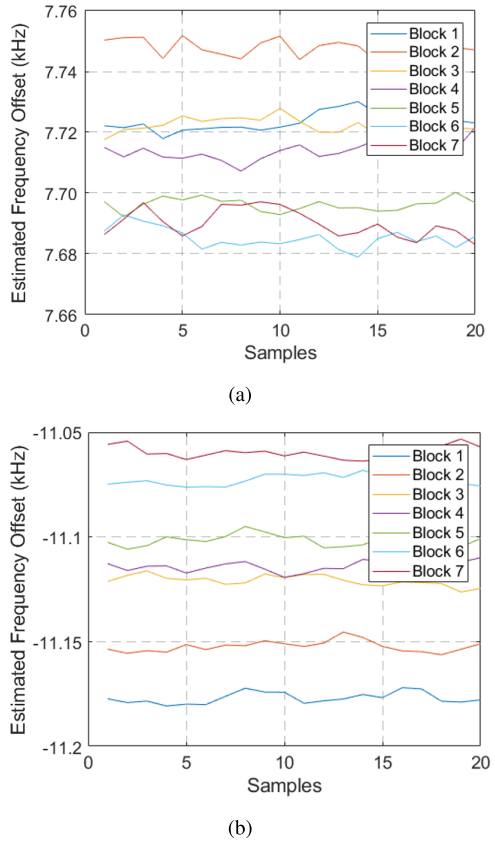

Fig. 6. Temporal variation of the estimated offset for one of the Twin A/D T.0X, during a 35s acquisition: a) before, and b) after processor restarting.

varied along the acquisition time with a maximum value of 70Hz; in each data block, the offset variation was lower than ±10 Hz. In Figure 6(b) the results obtained for the second acquisition of 35s are presented, showing the effect of the module restarting. In this case, the estimated frequency offset was −11.5KHz; the maximum difference between data blocks was 128Hz; in each data block, the offset variation was lower than ±10 Hz. For the other module of the same Twin A/D T.0X, the three estimated parameters (estimated frequency offset and inter and intra block variations) were quite different, as expected, because the modules of a Twin A/D T.0X operate independently.

A set of 12 Twin A/D T.0X processors were studied. Estimated output frequency offsets varied from few hundreds of Hz up to several tens of kHz, and changed every time the processors were switched on. These frequency offsets in the reference and surveillance channels of the PR give rise to artefacts in the CAF. The most relevant are the shift of stationary clutter's and stationary targets' contributions maxima to Doppler lines different from the zero one, and Doppler spread of these contributions due to time variations of the frequency offset. In Section III-D, a study of these CAF artefacts is presented using real data acquired by IDEPAR demonstrator after integrating the TWIN A/D T.0x processors.

D. Effects of Frequency Mismatching Modelling on PR

The model formulated in [26] is revisited, including the effects associated to the non-ideal performance of the proposed low cost recording system. For each DVB-T MX, and each CPI, the transmitted signal, $s_t(t)$, and the reference and surveillance signals at the antenna terminals, $s_r(t)$ and $s_s(t)$, are defined in (2), (3), and (4), respectively:

$$s_t(t) = a(t) \cdot cos(2\pi f_c(t) + \phi(t)) \tag{2}$$

$$s_r(t) = \xi_{A,r} \cdot a(t - t_L) \cdot cos(2\pi f_c t + \phi(t - t_L) \ldots - \phi_{c,r} + \xi_{\phi,r}) \tag{3}$$

$$s_s(t) = \xi_{A,s} \cdot a(t - t_T - t_R) \cdot cos[2\pi (f_c + f_D)t \ldots + \phi(t - t_T - t_R) - \phi_{c,s} - \phi_{D,s} + \xi_{\phi,s}] \tag{4}$$

where:

- $\xi_{A,r} \cdot e^{j\xi_{\phi,r}}$ is the complex gain factor for the reference signal, and the considered CPI, including propagation effects.
- $\xi_{A,s} \cdot e^{j\xi_{\phi,s}}$ is the complex gain factor for the surveillance signal, and the considered CPI, including propagation and scattering effects.
- f_c, $\phi_{c,r} = 2\pi f_c t_L$, and $\phi_{c,s} = 2\pi f_c(t_T + t_R)$ are the carrier frequency and phase delays.
- $f_D, \phi_{D,s} = 2\pi f_D t_R$, are the Doppler frequency and phase delay.

If the range origin is defined at the receiver, and the scatter echo delay is represented as $t_{sc} = t_T + t_R - t_L$, the new carrier and Doppler delays are defined as $\phi_c = 2\pi f_c(t_{sc})$ and $\phi_D = 2\pi f_D(t_R - t_L)$:

$$s_r(t) = \xi_{A,r} \cdot a(t) \cdot cos(2\pi f_c t + \phi(t) + \xi_{\phi,r}) \tag{5}$$

$$s_s(t) = \xi_{A,s} \cdot a(t - t_{sc}) \cdot cos[2\pi (f_c + f_D)t \ldots + \phi(t - t_{sc}) - \phi_c - \phi_D + \xi_{\phi,s}] \tag{6}$$

For a set of P MXs:

$$s_r(t) = \sum_{p=1}^{P} \xi^p_{A,r} \cdot a^p(t) \cdot cos(2\pi f_c^p t + \phi^p(t) + \xi^p_{\phi,r}) \tag{7}$$

$$s_s(t) = \sum_{p=1}^{P} \xi^p_{A,s} \cdot a^p(t - t_{sc}) \cdot cos[2\pi (f_c^p + f_D^p)t \ldots + \phi^p(t - t_{sc}) - \phi_c^p - \phi_D^p + \xi^p_{\phi,s}] \tag{8}$$

In the recording system, the set of MXs are shifted in frequency to carrier values denoted as $f^p_{c,sh}$, to generate a new set of consecutive MXs. Due to non-ideal performance of the different configurable frequency converters, carrier shift and phase errors are introduced: Δf_r^p, Δf_s^p, $\phi_r'^p$, $\phi_s'^p$ respectively. Defining $\phi^p_{T,r} = \xi^p_{\phi,r} + \phi_r'^p$ and $\phi^p_{T,s} = -\phi_c^p - \phi_D^p + \xi^p_{\phi,s} + \phi_s'^p$

$$s_r(t) = \sum_{p=1}^{P} \xi^p_{A,r} \cdot a^p(t) \cdot cos(2\pi (f^p_{c,sh} + \Delta f_r^p)t + \phi^p(t) + \phi^p_{T,r}) \tag{9}$$

$$s_s(t) = \sum_{p=1}^{P} \xi^p_{A,s} \cdot a^p(t - t_{sc}) \cdot cos[2\pi (f^p_{c,sh} + \Delta f_s^p + f_D^p)t \ldots + \phi^p(t - t_{sc}) + \phi^p_{T,s}] \tag{10}$$

After the recording system, received signals $s_r(t)$ and $s_s(t)$ are down converted to obtain the baseband

signals (11) and (12):

$$s_r(t) = \sum_{p=1}^{P} a^p(t) \cdot e^{j2\pi\phi^p(t)} \cdot \alpha_r^p(t) \cdot e^{j2\pi(f_{bb}^p + \Delta f_r^p)t} \quad (11)$$

$$s_s(t) = \sum_{p=1}^{P} a^p(t - t_{sc}) \cdot e^{j2\pi\phi^p(t-t_{sc})} \cdot \alpha_s^p(t) \cdot e^{j2\pi(f_{bb}^p + f_D^p + \Delta f_s^p)t} \quad (12)$$

where $\alpha_r^p = \xi_{A,r}^p \cdot e^{j2\pi\phi_{T,r}^p}$, $\alpha_s^p = \xi_{A_s}^p \cdot e^{j2\pi\phi_{T,s}^p}$ and f_{bb}^p is the MX baseband carrier frequency.

Equation (12) considers only the echo generated by a single scatterer in the area of interest; nevertheless, the signal model can be extend to $m = 1, \ldots, M$ scatterers (13).

$$s_s(t) = \sum_{p=1}^{P} \sum_{m=1}^{M} a^p(t - t_{sc}^m) \cdot e^{j2\pi\phi^p(t-t_{sc}^m)} \cdot \alpha_s^{p,m}(t) \ldots \cdot e^{j2\pi(f_{bb}^p + f_D^{p,m} + \Delta f_s^p)t} \quad (13)$$

Phase and frequency mismatchings between reference and surveillance signals will affect the coherent processing implemented by the CAF. To illustrate the problem to be faced, real radar signals acquired with IDEPAR after integrating the Televes A/D T.0X processors were analysed. For the experiment, a configuration with one reference and one single surveillance channel was selected. The reference antenna was pointed directly to the IoO and the surveillance one to an area of interest with moving targets, buildings, and other sources of clutter. The main signal contribution of the reference signal, $s_r(t)$, was the direct DVB-T broadcasted signal. The surveillance one, $s_s(t)$, was composed of Direct Path Interference (DPI) from the IoO, clutter and targets' echoes. In this case, the main power contributions come from DPI and clutter sources, being the power of targets' echoes up to 60dB lower, so Doppler effects produced by moving targets over the whole surveillance signal were negligible.

The system was configured to acquire a bandwidth of 25MHz centred at 850MHz. DVB-T MX at physical channel 58 (770MHz) was sifted to 850MHz by Televes processors. The CAF output was calculated for a CPI with $T_{int} = 250$ms. Clutter contributions maxima were found in the 1060Hz Doppler line (Figure 7), very far from the expected zero Doppler line. These effect is explained by the intra-CPI frequency variations of the Twin A/D T.0X modules included in (11) and (13).

To reduce, ideally suppress, these artefacts, an offset compensation stage before of the PR coherent processing is proposed. Each DVB-T MX shift requires two Twin A/D T.0X modules, one for the reference channel and another for the surveillance one. Due to the output frequency variations of the modules, frequency offset compensation must be applied to all the modules during all the PR operation time. Filtering techniques must be used to isolate each individual DVB-T MX from the reference and surveillance signals. After the offset compensation stage, both signals will be concatenated in the frequency domain to generate the multichannel signal to be processed by the PR.

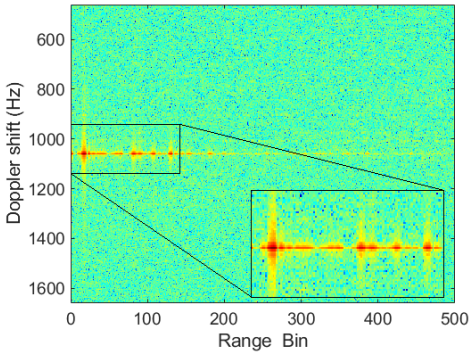

Fig. 7. CAF output generated using two conversion modules for shifting MX at physical channel 56 (770MHz) to 850 MHz.

Compensation algorithms must operate with input signal frequency mismatching up to 100kHz, under both direct path and multipath dominant channels. Frequency offset must be reduced up to PR Doppler resolution (4Hz in case of T_{int}=250ms) to center the maxima of stationary clutter contributions along the zero Doppler line and to ensure the correct interpretation of target' echoes. In addition, the compensation stage must minimize clutter Doppler spread, to limit targets' masking effects.

Commercial DVB-T signal reception requires time an frequency alignment techniques for decoding the OFDM modulated signal [32]. Multiple synchronization algorithms are available in the literature, exploiting dedicated preamble sequences [39], [40], pilot tones [41] or the cyclic prefix [42]. In section IV, the method described in [30] is analysed for the considered PR application, to define the basis for the design of the novel approach proposed in section V. The real radar signals studied above were also used to illustrate the operation principle of both algorithms.

After frequency alignment, carrier shifts' errors generated by the frequency converters, Δf_{rp}, will be significantly reduced, but phase mismatchings grouped in $\phi_{T,rp}$, $\phi_{T,sp}$ and target Doppler shifts will remain. In [26], an individual channel phase estimation is applied to each target after first detection and tracking stages based on a single MX. After that, the phase is compensated in the reference and surveillance signals before the multiple MXs coherent processing. Errors depend on the commercial modules operation, but also on channel propagation and target' position and complex reflection gain.

In this work, detection is performed on the multiple MXs signal after applying the frequency converters offset compensation algorithm proposed in Section V, and a multi-area CAF strategy is proposed for correcting target Doppler spread due to the different carriers that compose the signal (subsection VI.VI-A). A study is presented to analyse the influence of residual frequency and phase mismatchings using the low cost approach based on the frequency converters and a high performance reference processing architecture. The objective of this study is to distinguish the effect of carrier and targets' Doppler phase delays, associated to signal features and propagation effects, from residual errors by non-ideal receiver components. In both cases, the SNR is expected to be lower than when using a completely frequency and phase corrected

signal, but higher than when using a single MX. Once the suitability of the proposed low cost approach is proved, the reduction of residual frequency and phase mismatchings will be tackled in future works.

IV. Cyclic Prefix Van De Beek Method

The algorithm proposed in [30] is a common method for blind time and frequency synchronization of OFDM signals, based on a joint Maximum Likelihood (ML) estimator (14) of the symbol time beginning, θ, and the carrier frequency offset, ε, which exploits the redundancy of the cyclic prefix inherent to the OFDM signals, and the correlation characteristics.

$$\Lambda(\theta,\varepsilon) = |\gamma(\theta)|cos(2\pi\varepsilon + \angle\gamma(\theta)) - \rho\Phi(\theta) \tag{14}$$

$\gamma(\theta)$ is the sum of L correlations between the acquired signal $S(k)$ (composed of one single DVB-T MX from $s_{ref}[n]$ or $s_{surv}[n]$) and a copy delayed a number of samples, N, equal to the number of OFDM useful symbol samples; L is the cyclic prefix number of samples (15). $\Phi(\theta)$ is an energy term defined in (16) and ρ is a weighting-factor that depends on the Signal-to-Noise Ratio, SNR (17).

$$\gamma(\theta) = \sum_{k=\theta}^{\theta+L-1} S(k)\cdot S^*(k+N) \tag{15}$$

$$\Phi(\theta) = \frac{1}{2}\sum_{k=\theta}^{\theta+L-1} |S(k)|^2 + |S(k+N)|^2 \tag{16}$$

$$\rho = \frac{SNR}{SNR+1} \tag{17}$$

The maximization of (14) in both θ and ε dimensions, produces the ML estimation of the symbol time beginning, $\hat{\theta}_{ML}$, (18) and carrier frequency offset, $\hat{\varepsilon}_{ML}$, (19).

$$\hat{\theta}_{ML} = arg\,max_{\theta}(|\gamma(\theta)| - \rho\Phi(\theta)) \tag{18}$$

$$\hat{\varepsilon}_{ML} = -\frac{1}{2\pi}\angle\gamma(\hat{\theta}_{ML}) \tag{19}$$

Due to the periodicity of the cosine function in (14), this method can estimate carrier frequency offsets up to half sub-carrier frequency spacing. In Spain, the DVB-T symbol useful time, T_U, is $896\mu s$, so the sub-carrier frequency spacing is $1/T_U \simeq 1.11kHz$ and the compensable frequency error $\pm$0.55kHz. The frequency offsets produced by the recording system studied in section III-C can be several tens of kHz, so a pre-processing stage is required to reduce the frequency offset to the method limits. Techniques based on DVB-T channel active sub-carriers are normally used to limit the initial frequency offset to the sub-carrier spacing.

In Figure 8 the ML metrics are displayed for acquired reference and surveillance channels: ML time metric, $|\gamma(\theta)| - \rho\Phi(\theta)$, at the top, and ML carrier frequency offset metric, $-\frac{1}{2\pi}\angle\gamma(\theta)$, at the bottom. At the beginning of each OFDM symbol, the time metric produces a maximum value due to the integration of all the cyclic prefix contribution in the $\gamma(\theta)$ function. When the time metric reaches a maximum, the carrier frequency offset metric provides the value of the signal frequency offset estimation. The ML metrics variations

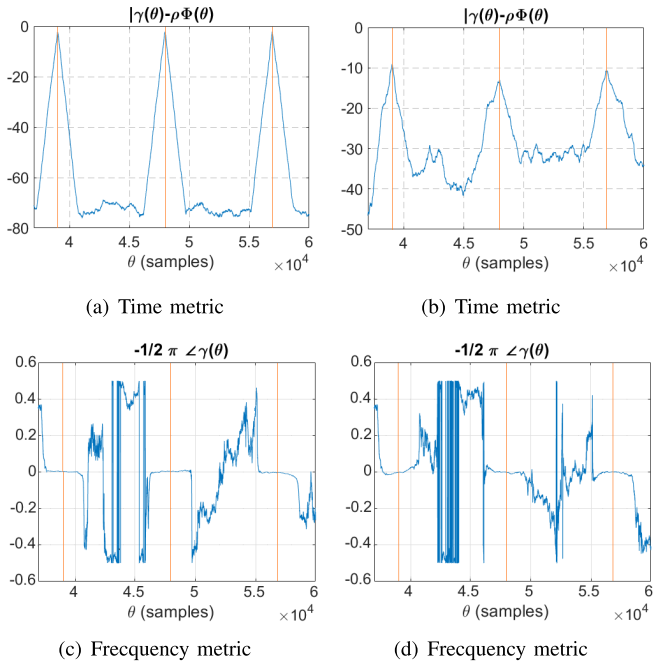

(a) Time metric (b) Time metric

(c) Frecquency metric (d) Frecquency metric

Fig. 8. Example of van de Beek metrics for ML estimation: reference (a,c) and surveillance (b,d) channels. OFDM symbol beginnings are marked by an orange line.

are different for the reference and the surveillance channels. In the reference channel, the time metric (Figure 8(c)) follows a clean shape with similar local maxima at consecutive symbol beginnings. On the other hand, the time metric of the surveillance channel (Figure 8(d)) shows a variable shape, with irregular slope, several sub-maxima around symbol beginnings and different distances between them. Nevertheless, thanks to the relative constant correlation phase along symbol beginnings, the proposed estimator can produce a relative low error decision. The pernicious effects on the PR surveillance channel frequency estimation process are explained by the multipath dominant signal, and its inherent lower SNR. In order to reduce the frequency estimation errors in the compensation stage, an average of the estimation obtained from the symbol beginnings into a CPI will be carried out.

The van de Beek algorithm provides good estimation results for the direct reception of DVB-T signals. Nevertheless, the multipath dominant scheme of the surveillance channel increases the estimation error. In section VI, this algorithm is applied to real data acquired by the IDEPAR demonstrator. Results show that reference and surveillance channels frequency mismatching can be reduced to be lower than the PR Doppler resolution (4Hz), but residual frequency errors produce Doppler spread of the main clutter sources, reducing system detection performance.

V. Proposed Offset Compensation Algorithm

The functional description of the proposed compensation technique is depicted in Figure 9. It includes a coarse offset compensation stage which limits the individual DVB-T MX offset to tens of Hz with respect to the theoretical channel central frequency, and a fine adjustment stage, which shifts

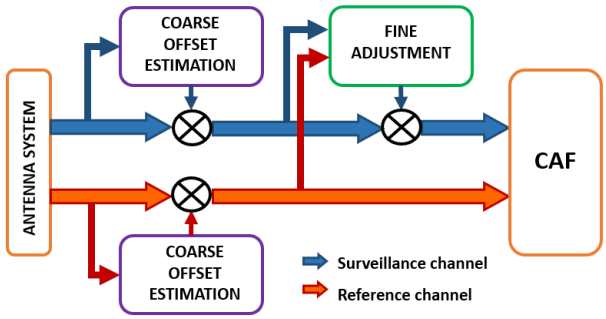

Fig. 9. Functional description of the proposed offset compensation scheme.

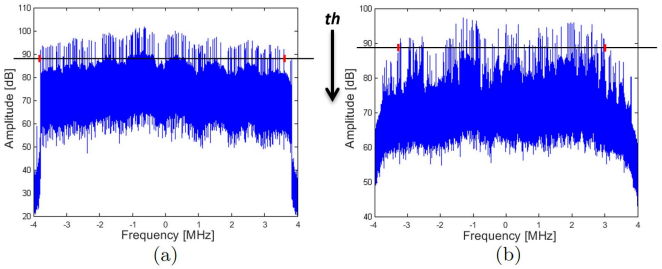

Fig. 10. DVB-T channel bandwidth estimation process for the reference (a) and the surveillance (b) signals.

the surveillance DVB-T MX to match with the actual central frequency of the reference one.

A. First Stage: Coarse Offset Estimation

This stage compensates the difference between the central frequency of the signal provided by the Twin A/D T.0X module and its selected output, limiting the frequency difference up to tens of Hz. The estimation process is carried out in the frequency domain by means of the DFT of a CPI from each acquired DVB-T MX. The coarse offset estimation process is divided into the followings steps:

Spectral averaging: To improve the frequency estimation capabilities, the spectral average between consecutive CPIs is calculated.

Central frequency search: The algorithm works as a recurrent process that calculates the signal bandwidth, $BW(th)$, over a variable threshold, th, and its associated central frequency, $fc(th)$, (Figure10). The value of this threshold begins 10dB below the maximum signal level and decreases in each iteration 0.2dB. The relations between the estimated signal bandwidth and the threshold level for the reference and surveillance signals are depicted in Figure 11. In case of the reference signal, the theoretical DVB-T channel bandwidth (7.6071MHz) matches the estimated one for many threshold levels due to the high SNR. In contrast, the surveillance signal spectrum has a lower signal level and irregular shape that makes the estimation of the DVB-T channel bandwidth difficult. To avoid the pernicious effects of the channel dispersion and power level differences, all the estimated bandwidths in the interval 7.6071MHz $\pm$ 50Hz are selected, and the final frequency shifts, $\hat{\Delta} f_i^p$ ($\hat{\Delta} f_r^p$, for the reference channel

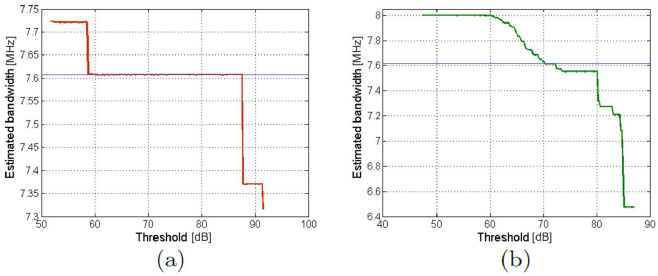

Fig. 11. Example of estimated bandwidth vs. threshold: a) reference channel; b) surveillance channel. The theoretical bandwidth is represented as a blue line.

and $\hat{\Delta} f_s^p$ for the surveillance one), are computed in (20) subtracting the mean value of the central frequencies of the selected estimated bandwidths, from the desired baseband central frequency, f_{bb}^p. An average between the actual offset estimation and the previous ones is applied. This process reduces considerably the associated error when the level of the DVB-T spectrum is close to the noise floor, enabling the correct operation of the remaining offset compensation steps.

$$\hat{\Delta} f_i^p = f_{bb}^p - mean(fc(th) \forall th \,|\, BW(th) \in [7.6071 \cdot 10^6 \pm 50]) \quad p = 1, \ldots, P \text{ and } i \in [r, s] \tag{20}$$

Offset compensation: Frequency shifts, $\hat{\Delta} f_r^p$ and $\hat{\Delta} f_s^p$ are compensated in each isolated MX, $p = 1 \ldots P$. Estimation errors give rise to a residual frequency mismatching, $\varepsilon'^p = \varepsilon_s^p - \varepsilon_r^p$, that requires a fine adjustment in the second stage of the algorithm (21)-(22)

$$s_r'(t) = \sum_{p=1}^{P} a^p(t) \cdot e^{j2\pi\phi^p(t)} \cdot \alpha_r^p(t) \cdot e^{j2\pi(f_{bb}^p + \varepsilon_r^p)t} \tag{21}$$

$$s_s'(t) = \sum_{p=1}^{P} \sum_{m=1}^{M} a^p(t - t_{sc}^m) \cdot e^{j2\pi\phi^p(t - t_{sc}^m)} \cdot \alpha_s^{p,m}(t) \ldots \cdot e^{j2\pi(f_{bb}^p + f_D^{p,m} + \varepsilon_{ref}^p + \varepsilon'^p)t} \tag{22}$$

where $\varepsilon_r^p = \Delta f_r^p - \hat{\Delta} f_r^p$ and $\varepsilon_s^p = \Delta f_s^p - \hat{\Delta} f_s^p$.

B. Second Stage: Fine Adjustment

The algorithm modifies the central frequency of the surveillance channel, towards the current value of the reference one, minimizing the residual frequency mismatching, ε'^p. The fine offset compensation stage is divided into the followings steps:

- **Zero Doppler line positioning:** The differences between reference and surveillance channels can be of tens of Hz. To limit the offset error to the PR resolution, a process based on the CAF is used. The value of the Doppler row that presents the highest level (associated with clutter contributions), is used for the surveillance channel but with opposite sign. The system Doppler resolution will be the maximum accuracy achievable in this step, $\Delta_{fDoppler}$=4Hz for T_{int}=250ms
  Although the stationary clutter contributions maxima are positioned along the zero Doppler line, a Doppler spread

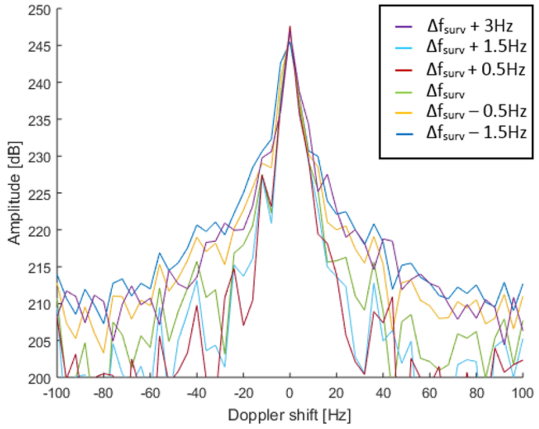

Fig. 12. Example of CAF output main clutter cut along Doppler dimension for six shifted copies of the surveillance channel.

can appear due to the residual frequency mismatch. This dispersion can affect the detection capabilities.

- **Focusing stage:** In order to break through the accuracy limitation of the previous step, an optimization recursive algorithm based on multiresolution techniques is proposed:
  1) First iteration of the optimization algorithm:
  Definition of the initial search grid: A set of five frequency offsets are selected at each side of the zero Doppler line estimated in the *zero Doppler line positioning* step. These frequencies are defined as $f_{search,1} = -5 + l,\ l \in \{0, 1, \ldots, 10\}$. For each frequency of the grid, a shifted copy of the surveillance channel and its associated short range CAF output are obtained (S_l^{CAF}).
  The main clutter source column is selected as a representative sample of the Doppler spread in each CAF output. In Figure 12, the level distributions on this column for a set of six surveillance frequency offsets are displayed.
  Definition of a new cost function in the CAF domain to be minimized (23). It is calculated as the difference between the pedestal and the zero-Doppler position levels in the range column belonging to the main source of clutter.

$$C(l) = -2S_l^{CAF}[\lfloor R/2 \rfloor, j] + \sum_{i=0}^{R} S_l^{CAF}[i, j] \quad (23)$$

  S_l^{CAF} is the CAF of the reference signal compensated in the first stage, and the surveillance one shifted to each search frequency defined by $f_{search,1}(l)$, being R the number of CAF rows and j the column of the main clutter source. The search frequency associated to the minimum value of the cost function is selected and denoted as $f_{zero,1}$.
  2) Subsequent iterations: In the $i-th$ iteration, $i > 1$, a new search grid is defined centred on $f_{search,i} = f_{zero,(i-1)} + ((-5+l)/(5i-1)),\ l \in \{0, 1, \ldots, 10\}$. The cost function is recalculated to determine the frequency that minimizes its value: $f_{zero,i}$.
  3) Stopping criterion: The iterative process will stop when the cost function decrease is lower than 0.1% in two consecutive iterations.

After last iteration, the pair of reference and surveillance channels with lowest dispersion are selected as algorithm output to continue the radar processing stages.

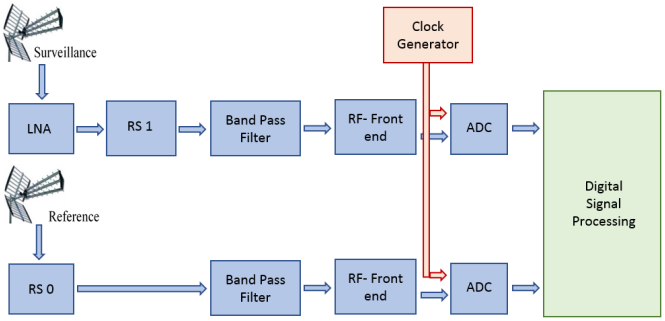

Fig. 13. IDEPAR acquisition chain after the recording system integration. Each RS is composed of two Twin A/D T.0X.

VI. Results

A. Case Study

To test the proposed low cost recording system and the compensation algorithms capabilities, real passive radar data were used. The Twin A/D T.0X. processors were integrated in the IDEPAR demonstrator [16]. Two Twin A/D T.0X working in parallel were needed in each receiving chain to shift three DVB-T MXs into a 24MHz bandwidth centred at 850MHz, where the bandpass filter operates to limit the noise before the digitalization process. In the surveillance channel, the low noise amplifiers were placed after the antenna element in order to ensure the input minimum level of the Twin A/D T.0X mixers. The reference acquisition chain was similar to the surveillance one without the LNAs due to the reception of the direct signal from the IoO. In Figure 13 the block diagram of the new acquisition chain is shown.

The new version of IDEPAR was tested in a semi-urban scenario placed in the vicinity of the Superior Polytechnic School (SPS) of the University of Alcalá (Figure 14). The PR demonstrator was placed in a elevated position in the building roof. The surveillance antenna element was pointed to a relative open area at the North of the radar location with big buildings at both sides: the SPS on the left and a big metallic building on the right (IMMPA). The area of interest was composed of two roads where moving cars and lorries were expected: the R2 highway and the Meco road. Torrespaña DVB-T transmitter, located 28km faraway, was selected as IoO due to its high power and transmitted MXs.

Two real data sets were acquired, one for the analysis of the proposed low-cost system, and the other for the comparative analysis of compensation algorithms. In both sets, the processors were configured to shift the DVB-T MXs at physical channels 55, 58 and 59, whose central frequencies were 746, 770 and 778 MHz, in a 24MHz consecutive bandwidth centred in 850MHz.

A high performance acquisition system based on USRP X310 mounting twinRX daugther-boards was selected as

(a)

(b)

(c)

Fig. 14. Top view of the PR scenario (a) and new version of IDEPAR (reference antenna with the commercial recording system (b), rack front-side view (c)): the area of interest (dark green) is composed of segments of the R2 highway (blue) and Meco road (yellow). The presence of the SPS and IMMPA building sections inside the area of interest may cause big reflections and shadowed areas.

reference for the low cost system performance analysis. The X310 solution was configured to acquire a 50MHz bandwidth centred at 762MHz to be able to digitalize the three disperse DVB-T MXs selected in the radar scenario (with central frequencies 746, 770 and 778 MHz). Digital processing techniques were applied to select and frequency shift the acquired MXs to consecutive baseband positions. The first real data set is the result of 10s simultaneous acquisitions using the low cost proposed solution and the high performance reference one. Acquired signals were divided into 40 CPIs of $T_{int} = 250$ms. Systems' performances were compared in terms of system resolution and targets' echo SNR (Subsection VI.VI-B).

A second acquisition was performed by the low cost proposed solution with $T_{acq} = 30$s. Signals were processed in CPIs of $T_{int} = 250$ms, giving rise to 120 CPIs with a Doppler resolution $\Delta_{fDoppler} = 4$Hz. The following methodology was applied for the comparative analysis of the van de Beek compensation algorithm, and the one proposed in this article (Subsection VI.VI-C):

- **First compensation stage:** the coarse offset estimation process described in section V.V-A was applied to each DVB-T MX of the reference and surveillance signals, in order to compensate the main offset component.
- **Second compensation stage:** the two fine compensation methods described in this work were applied to the preprocessed signals: Cyclic prefix van de Beek method and the proposed fine adjustment algorithm.
- **Preprocessing stage:** To reduce the effects of clutter and DPI, an adaptive filtering technique based on fast Extensive Cancellation Algorithm (ECA) was applied [43].
- **Coherent processing stage:** the initial frequency gap between DVB-T MXs can produce different target's Doppler frequencies. If this difference exceeds the Doppler resolution, the target's echo is separated into different Doppler cells. To concentrate the target's echo at the same Doppler cell, the RDM is divided into Doppler areas where different CAFs are computed. In the central area (low target's velocities) no Doppler division is expected, so the CAF is computed with non-modified reference and surveillance channels. In the adjacent areas, the frequency of the separated DVB-T MXs in the surveillance signal is modified in steps equal to the system Doppler resolution before the CAF, to concentrate the target's contributions at the same Doppler cell. For the selected DVB-T MXs, a 4Hz Doppler change every 97.25Hz and a maximum ground target Doppler of 120Hz are expected. Therefore, a solution based on three RDM areas is performed.
- **Detection stage**: to compare the effects of the compensation algorithms, a square-law envelope detector and a Cell-Averaging Constant False Alarm (CA-CFAR) technique were applied using a bi-dimensional window extended along 21 range cells and 13 Doppler ones, with 2 guard cells along each dimension and a designed $P_{FA} = 10^{-6}$ [16].
- **Detection performance analysis**: Probability of Detection (P_D) and Probability of False Alarm (P_{FA}) values were estimated using the methodology detailed in [16]. The P_D was calculated at plot level due to the errors associated with the pixel detection grouping techniques, generating common ground-truths for each declared target using the target information provided by a Kalman filter based tracker. On the other hand, P_{FA} was estimated at pixel level in the CAF areas where no targets are expected. Monte-Carlo simulations with an estimation error lower than 10% were used.

B. Proposed Low Cost Vs. High Performance Reference Solution. Comparative Study

The first real data set was used for this study (three disperse DVB-T MXs located at 746 MHz, 770 MHz and 778 MHz carriers):

- Low cost approach: The Televes processors include high selectivity Surface Acoustic Wave (SAW) filters, with impedance matching networks and low noise amplifiers to compensate the high insertion losses (21 dB), giving rise to a high selectivity solution with an equivalent noise degradation lower than 2dB. The final signal applied to the acquisition system has a bandwidth of 24MHz composed of the 3 filtered and frequency shifted signals. Carrier offset and target Doppler compensation techniques presented in this article were applied to the digital signal.
- Reference solution, which is configured to acquire a continuous bandwidth of 50MHz. Daughter-boards

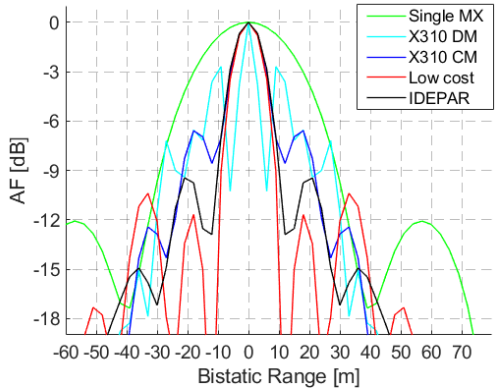

(a)

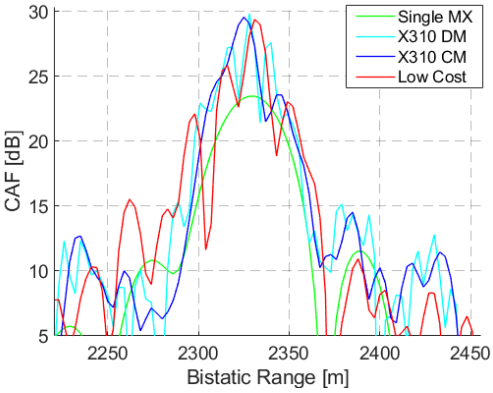

(b)

Fig. 15. Acquisition system performance comparison: a) AF zero-Doppler cut; b) CAF cut along bistatic range at non-cooperative target echo position.

pre-selectors stage is composed of a set of 8 band-pass filters. For the three non-consecutive MX DVB-T signals, the band-pass filter extends from 500MHz to 800MHz, with insertion losses of approximately 3.5dB. After two frequency conversion stages, the signal centred at 150MHz with 80Mz bandwidth is applied to the ADC. The final 50MHz filter is implemented digitally. After that, high selectivity digital filters were applied to isolate the DVB-T MXs. Different signals were generated: a single MX (Single MX), three disperse MXs (X310 DM), and three disperse MXs, reallocated to consecutive frequency positions (X310 CM).

In both cases, signals were resampled at 100 MHz to analyse bistatic range resolution using the AF. Figure 15(a) shows the AF zero Doppler for the four defined cases and a fifth one using three consecutive MXs acquired by IDEPAR demonstrator before the DVB-T reallocation process (IDEPAR). In all cases, the estimated bistatic range resolutions exceed the individual DVBT MX one. Nevertheless, the presence of bandwidth gaps in the X310 DM signals produces a modulation of the compressed pulses with a reduction of the main lobe width, and high side lobes that could affect the detection stage. In consecutive MXs cases (X310 with digital relocation, the proposed solution and the previous IDEPAR acquisition chain) the side-lobe levels decrease and the bistatic range resolution approach the theoretical value for three DVB-T MXs (13.16m).

TABLE II
NON-COOPERATIVE TARGET BISTATIC RANGE EXTENSION AT HALF POWER

	Best MX	X310 DM	X310 CM	Low Cost
Target 1	42.6 m	22.4 m	21.9 m	23.2 m
Target 2	40.8 m	22.5 m	20.4 m	22.8 m
Target 3	36.2 m	18.9 m	18.9 m	20.2 m

TABLE III
NON-COOPERATIVE TARGET SNR COMPARISON

	Best MX	X310 DM	X310 CM	Low Cost
Target 1	14.17 dB	16.33 dB	16.56 dB	17.55 dB
Target 2	22.73 dB	24.46 dB	24.57 dB	24.91 dB
Target 3	29.82 dB	31.63 dB	31.87 dB	32.30 dB

Target echoes from different DVB-T MXs reach the PR location with different phase shifts (7-8). In the proposed low cost solution, phase shifts are added because of the non-ideal performance of the commercial frequency converters (9-10). Figure 15(b) shows cuts of the CAF in the CPI 6 at the echo position of a detected target. The CAF outputs are normalized by their noise pedestal level to represent the SNR for each acquisition architecture. Non-compensated initial phases, $\phi^p_{T,r}$ and $\phi^p_{T,s}$, negatively affect system performance, generating relative maxima close to the AF peak. A variation of the AF peak position is also observed. These effects increase when the carrier differences between the acquired DVB-T MXs are kept (X310 DM case). The 3dB width of the target radar echo along the bistatic range dimension was analysed for three non-cooperative targets. Mean values estimated along the whole acquisition time for all study cases are summarised in Table II. Results show a reduction of the 3dB width of the target echo along bistatic range by a factor of 2 when the three DVB-T MXs are considered. The increase of the bandwidth also increases the SNR of the target at the input of the detection stage. Table III summarizes the mean SNR estimated for three targets along the whole acquisition time. The use of multiple sparse or reallocated DVB-T MXs improves targets' SNR with respect to the use of a single MUX. Due to the effects of phase distortion, the theoretical improvement is reduced from 4.78 dB to approximately 2.5dBs. SNRs estimated for the proposed low-cost architecture are comparable to those obtained from the X310 based solutions, with an increase lower than 1dB in the best case, that can be related to non-ideal behaviour of the different processing chains. In any case, results prove the good performance of the proposed carrier offset and target Doppler compensation techniques. In the three cases (X310 DM, X310 CM and Low Cost) target SNR is up to 3dB better than the best single DVBT MX.

Acquired data were digitally separated into blocks of 2MXs to analyse system performance for consecutive and disperse MXs. Two case studies were defined for both high quality X310 devices based, and low cost approaches: acquisition of two consecutive MXs (DVB-T physical channels 58 and 59), and acquisition of two disperse MXs with 16MHz of separation (DVB-T physical channels 55 and 58). Figure 16 depicts the CAF cut at target location for CPI 6 and for

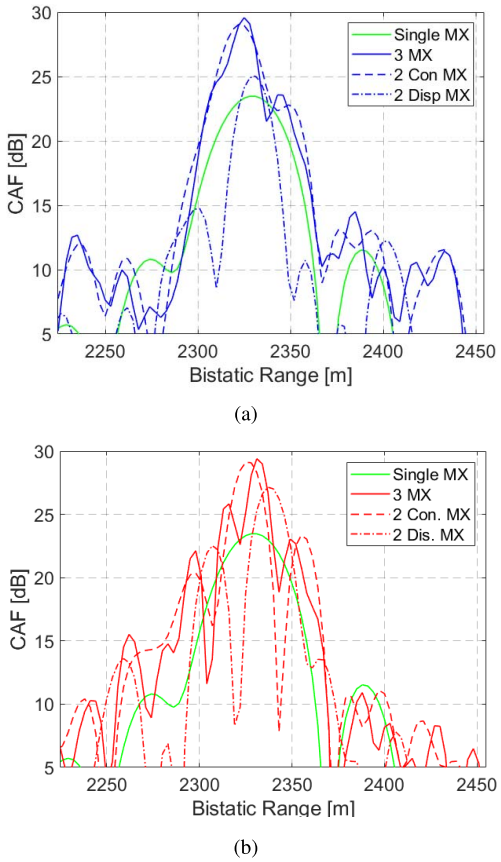

Fig. 16. CAF cut along bistatic range at non-cooperative target echo position. Comparison between two consecutive and disperse MXs for both processing scheme: a) X310; b) and low cost.

TABLE IV
TARGET BISTATIC RANGE EXTENSION AT HALF POWER COMPARISON BETWEEN TWO CONSECUTIVE AND DISPERSE MXS FOR BOTH PROCESSING SCHEMES (X310 AND LOW COST)

	X310		Low Cost	
	Con. MX	Dis. MX	Con. MX	Dis. MX
Target 1	25.6 m	33.4 m	27.2 m	33.0 m
Target 2	24.5 m	29.4 m	28.8 m	31.65 m
Target 3	22.8 m	27.9 m	27.6 m	25.35 m

both approaches. The 2MXs consecutive (Con.MX) and disperse (Dis.MX) cases are compared with the previous three MXs and single MX cases. The estimated non-cooperative target bistatic range extension measured between half power points along the whole acquisition is presented in Table IV. Results show a lower target extension when consecutive MXs are considered, especially in the high quality solution, due to the absence of frequency and phase distortions produced by the commercial modules. Nevertheless, the solutions based on three non-consecutive DVB-T MXs for both low cost and high quality systems, improve system performance compared with that obtained processing 2 consecutive MXs.

Despite of the extra phase distortion due to the use of commercial modules, the proposed low cost solution provides similar resolution and SNR performances than those obtained by high performance acquisition boards. To approximate the theoretical system performances, echo phase compensation methods will be studied in future works.

TABLE V
DVB-T MXS COARSE OFFSET ESTIMATION

	DVB-T Physical Channel		
	55	58	59
Reference	-868 Hz	4764 Hz	1827 Hz
Surveillance	2350 Hz	2176 Hz	2620 Hz

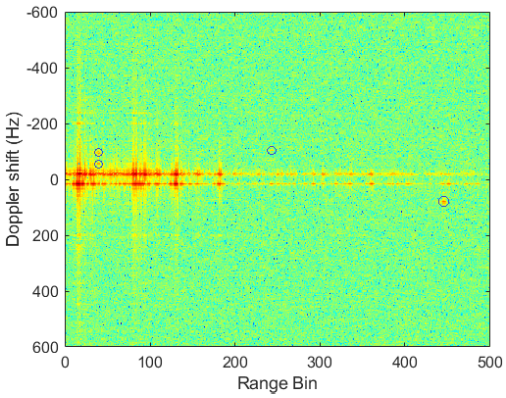

Fig. 17. CAF output of the 60th CPI after the application of the coarse offset compensation process. Residual frequency mismatching produces Doppler shifts in clutter and DPI contributions. Blue circles indicate target positions.

C. Frequency Alignment Algorithms Comparison

1) Coarse Offset Estimation: The estimated frequency shifts of the three DVB-T MXs with the coarse offset estimation stage, in both reference and surveillance signals, are summarized in Table V. All reference channel CPIs are correctly processed due to the high signal level (from 20dB to 55dB, which is lower than the 86.04dB provided by the acquisition boards, Section VI.VI-A). The lower surveillance channel SNR (from 5dB to 22dB) and multiple source signals (targets, DPI and clutter), only allow the correct processing of some of the CPIs. In Figure 17 the CAF generated from the 60th CPI after the coarse offset estimation stage is shown. DPI and ground clutter contributions maxima are visible around the theoretical zero Doppler position, at -24, -20 and 16 Hz for each DVB-T MX pair. The residual frequency mismatching is also represented by the clutter contribution spread along Doppler dimension. In addition, several target echoes can be differentiated in both near and far range. Nevertheless, useful radar information cannot be extracted due to their non-real location and movement characteristics. After the coarse estimation step, the frequency mismatching was reduced to several tens of hertzs, allowing the application of the van de Beek method and the one proposed in this article.

2) Comparative Analysis of the Fine Compensation Methods: In Figure 18, the CAF outputs after the whole compensation processes are displayed for the cyclic prefix van de Beek method, Figure 18(a), and proposed compensation algorithm, Figure 18(b). At this point, the preprocessing stage is not applied in order to evaluate the compensation methods behaviour based on clutter dispersion along Doppler dimension.

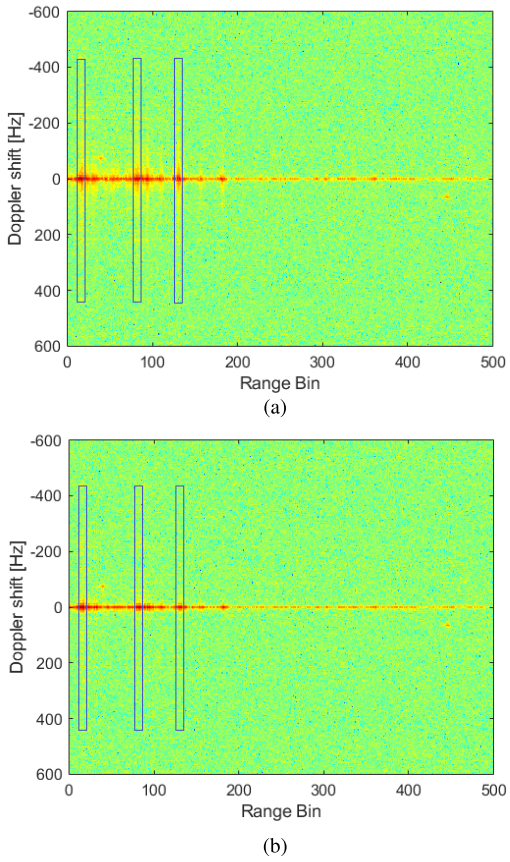

Fig. 18. RDM of the 60th PRI after the application of both compensation algorithms under study: a) cyclic prefix van de Beek method; b) proposed compensation algorithm. Blue rectangles denote the three main clutter sources for dispersion analysis.

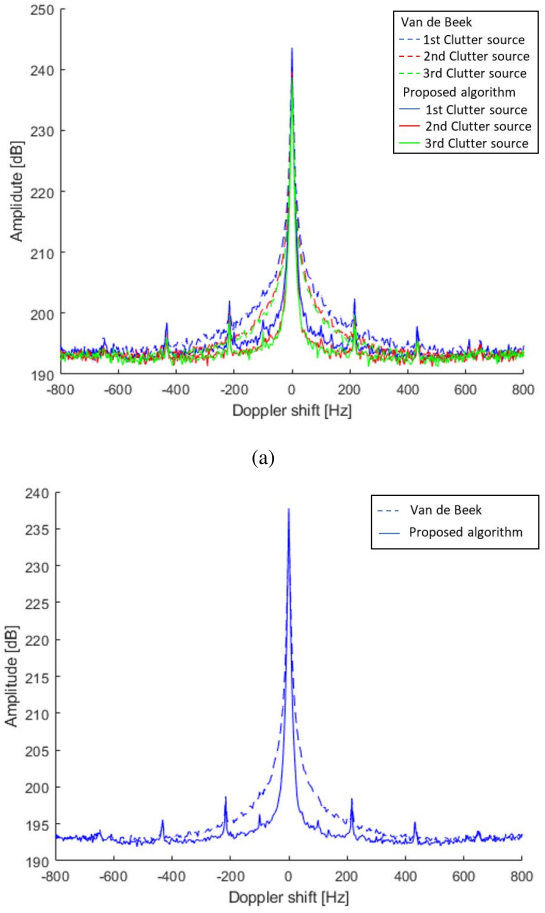

Fig. 19. a) Dispersion on the Doppler column at the three main clutter contribution positions; b) Mean dispersion between the selected columns (van de Beek method in discontinuous line, and the proposed compensation method in continuous line).

In both cases, DPI and ground clutter contributions maxima are correctly located along the zero Doppler line, but important differences can be appreciated. In the case of the van de Beek method (Figure 18(a)), a clutter power dispersion in the Doppler dimension is shown along all the zero Doppler line, being remarkable at the positions of the surrounding big buildings. At these range locations, the clutter power dispersion can shadow the moving targets, reducing radar detection capabilities. On the other hand, the proposed compensation algorithm concentrates DPI and ground clutter contributions maxima along the two Doppler bins close to the zero Doppler line with significantly lower dispersion effects along the Doppler dimension. In Figure 19, a study of the power spread along Doppler dimension for main clutter sources is shown. The compensation behaviour of both methods is similar in the extremes of the Doppler axis and the differences grow for Doppler values approaching to zero.

To study the dispersion effects on the radar performances taking into account all processing stages, the Signal to Interference Ratio (SIR) of different targets was analysed along the acquisition time. These targets were controlled by visual inspection during the acquisition time. To characterize this effect along different range areas, targets at three different locations were selected: two moving away from the PR receiver, starting in the 34 and 236 range bins, and one approaching to the radar location beginning in bin 447. The SIR level was analysed using a 2D window with two guard bins along range and Doppler dimensions, six reference cells to estimate the pedestal level, and the highest target echo. The mean value of the SIR along the acquisition time for the three targets is presented in table VI. A SIR improvement higher than 3 dB is obtained with the proposed method for two of the three considered targets. It affects the closest targets because high clutter contributions concentrate in the CAF area were these targets are detected. Although the first one is far from the zero Doppler line, clutter dispersion along Doppler is increasing the interference level in the reference cells used for SIR estimation.

TABLE VI
MEAN VALUE OF SIR FOR THREE TARGETS

Algorithm	Target 1	Target 2	Target 3
van de Beek method	13.05	14.57	27.45
Proposed compensation	16.96	17.99	28.11
Difference	3.91	3.42	0.66

The cumulative detection maps after the application of the square-law envelope detector and the CA-CFAR technique to

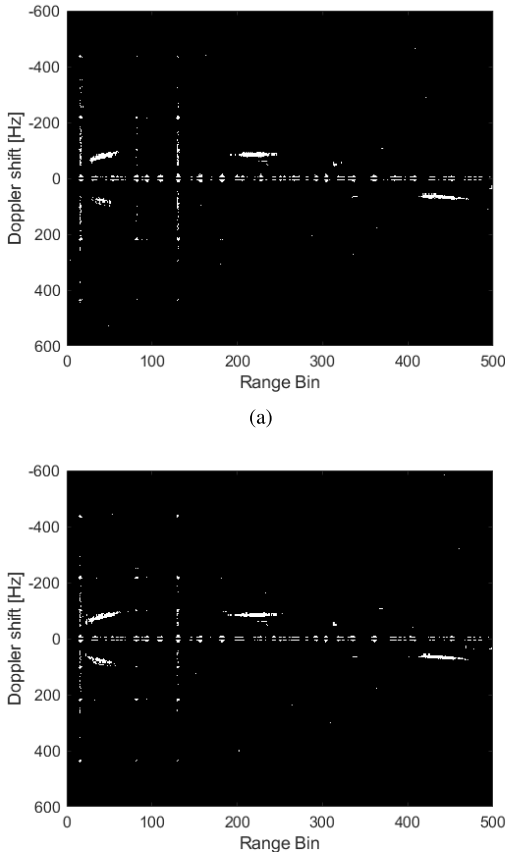

Fig. 20. Cumulative detection maps for 30 seconds of acquisition time: a) cyclic prefix van de Beek method; b) proposed compensation algorithm.

TABLE VII
ESTIMATED P_D AND P_{FA}

Algorithm	P_D	P_{FA}
van de Beek method	0.621	$7.34 \cdot 10^{-6}$
Proposed compensation	0.788	$7.46 \cdot 10^{-6}$
Diference	0.167	$-0.12 \cdot 10^{-6}$

the 120 CPIs are depicted in Figure 20. The signal filtering stage reduces the clutter and DPI presence in the surveillance channel, eliminating the false alarms at the zero Doppler-line and reducing the mean pedestal level approximately 1.5dB. Nonetheless, the clutter dispersion along Doppler dimension was not eliminated. Therefore, multiple detections are concentrated along lines closed to the zero Doppler. The influence of the clutter spread is also represented by means of recurrent false alarms along the columns of the three main clutter sources. The Doppler shifts of these false alarms agree with the local maxima of the clutter dispersion at 100, 216 and 432 Hz shown in Figure 19. In terms of false alarm rate, both compensation methods obtain similar results (Table VII), with a difference lower than the estimation error. In both cases, the estimated P_{FA} exceeds the design P_{FA} of 10^{-6} due to the presence of the aforementioned clutter spread. The differences between methods appear when the target detection capabilities are analysed (Table VII). Taking into account all available targets, the proposed compensation method allows a P_D improvement of 16.7%. The improvement increases to 25% when only the nearby targets, up to 100 range bins, are analysed. The influence of powerful clutter sources in this area is determining. The conclusions obtained in SIR analysed above are now evidenced. The detection trajectories generated for target 3 are similar: the proposed method allows its detection in 96 CPIs, whereas the van de Beek method obtains detections in 95 CPIs. In the trajectory estimated for target 2, target contributions concentration along the Doppler dimension is more visible. Target 1 contributions are located between the contributions of two powerful clutter sources. Using the proposed method, the target is detected in 48 CPIs, whereas with the van de Beek method, it is only detected in 38 CPIs.

VII. Conclusion

In this article, a commercial low cost solution to increase DVB-T based PR range resolution is presented and analysed. The possibility of using consecutive DVB-T MXs to increase signal bandwidth is an attractive possibility, but DVB-T MX allocation is characterized by a high spatial variability and frequency sparsity. The proposed solution is based on that proposed in [20]-[23] and allows the exploitation of multiple non-consecutive DVB-T MX from a single IoO, generating a new spectrum composed of consecutive shifted channels with a predefined guard band. The acquisition scheme of IDEPAR demonstrator was updated to include a new recording system in charge of the channels relocation. Following the COTS principles of the IDEPAR demonstrator, commercial Televes DVB-T modules were selected. The new hardware allows the selection of the channel to be shifted and the new central frequency, guaranteeing PR robustness with respect to DVB-T MX availability, and the fulfilment of requirements imposed by acquisition systems of operating systems (central frequency and signal bandwidth). But this hardware introduces frequency and phase mismatching between reference and surveillance channels that compromises system operation. To face channel central frequency variations, a CAF dispersion based compensation algorithm was proposed. The method was divided into two stages: a coarse offset estimation to enclose the shifted DVB-T MX around the desired center frequencies; and a fine adjustment that compensates the center frequency residual mismatching between reference and surveillance channels. The proposed low cost solution was evaluated in two levels: by the comparison with a high performances acquisition system and by the comparison between frequency compensation algorithms under the low cost acquisition system.

A high performances acquisition system based on USRP X310 capable of acquiring 80MHz of instantaneous bandwidth was selected as reference one. Systems performance was evaluated in terms of range resolution and target echo SNR. A simultaneous acquisition with the same three DVB-T MXs was carried out. Results show an almost equivalent range resolution and SNR improvement with both architectures with respect to a single DVB-T MX digitally isolated from the reference acquisition system.

To evaluate the performances of the proposed frequency compensation algorithm, the well-known cyclic prefix van de

Beek method was also applied to face frequency alignment. Although it was not designed for passive radar applications, is a reference solution to evaluate the proposed method's contributions in the considered applications. The performances of both algorithms were evaluated in terms of target SIR and clutter dispersion after CAF processing stage, and at detection level after the CA-CFAR detector. Results show a significant reduction of clutter dispersion when the proposed compensation algorithm was applied. The Doppler dispersion was mainly enclosed to an area of 20Hz around zero-Doppler line. According to target echo behaviour, all targets under study improved their estimated SIR, being the most relevant increase in the targets at low and medium distances where main clutter sources contributions concentrated. The combination of both effects produced significant detection capabilities improvement in areas near to the main clutter sources, as well as in the faraway targets where the clutter power decreases.

REFERENCES

[1] *IEEE Standard for Radar Definitions*, Standard 686-2017, Revision of IEEE Std 686-2008, 2017, pp. 1–54.

[2] P. Howland, "Editorial: Passive radar systems," *IEE Proc. Radar, Sonar Navigat.*, vol. 152, no. 3, pp. 105–106, Jun. 2005.

[3] A. Farina and H. Kuschel, "Guest editorial special issue on passive radar (part I)," *IEEE Aerosp. Electron. Syst. Mag.*, vol. 27, no. 10, p. 5, Oct. 2012.

[4] R. Klemm, U. Nickel, C. Gierull, P. Lombardo, H. Griffiths, and W. Koch, Eds., *Novel Radar Techniques and Applications Real Aperture Array Radar, Imaging Radar, and Passive and Multistatic Radar*. vol 1. London, U.K.: Institution of Engineering and Technology, 2017.

[5] K. E. Olsen and H. Kuschel, "From the editors of the special issue: Passive and multi-static radar for civil applications," *IEEE Aerosp. Electron. Syst. Mag.*, vol. 32, no. 2, p. 3, Feb. 2017.

[6] H. D. Griffiths and N. R. W. Long, "Television-based bistatic radar," *IEE Proc. F-Commun., Radar Signal Process.*, vol. 133, no. 7, pp. 649–657, Dec. 1986.

[7] P. E. Howland, D. Maksimiuk, and G. Reitsma, "FM radio based bistatic radar," *IEE Proc. Radar Sonar Navigat.*, vol. 152, no. 3, pp. 107–115, Jun. 2005.

[8] M. Malanowski, K. Kulpa, and J. Misiurewicz, "PaRaDe–PAssive RAdar DEmonstrator family development at Warsaw University of Technology," in *Proc. Microw., Radar Remote Sens. Symp.*, Sep. 2008, pp. 75–78.

[9] C. J. Coleman, R. A. Watson, and H. Yardley, "A practical bistatic passive radar system for use with DAB and DRM illuminators," in *Proc. IEEE Radar Conf.*, May 2008, pp. 1–6.

[10] R. Zemmari, U. Nickel, and W. Wirth, "GSM passive radar for medium range surveillance," in *Proc. Eur. Radar Conf. (EuRAD)*, Sep. 2009, pp. 49–52.

[11] D. Petri, A. Capria, M. Martorella, and F. Berizzi, "Ambiguity function study for UMTS passive radar," in *Proc. 2009 Eur. Radar Conf. (EuRAD)*, 2009, pp. 41–44.

[12] R. Saini and M. Cherniakov, "DTV signal ambiguity function analysis for radar application," *IEE Proc.-Radar, Sonar Navigat.*, vol. 152, no. 3, pp. 133–142, Jun. 2005.

[13] D. W. O'Hagan, P. Knott, M. Simeoni, M. Schröder, V. Basavarajappa, and H. Kuschel, "Wideband antenna array for digital video broadcast terrestrial-based passive bistatic radar applications," *IET Radar, Sonar Navigat.*, vol. 8, no. 2, pp. 106–113, Feb. 2014.

[14] M. Conti, F. Berizzi, M. Martorella, E. D. Mese, D. Petri, and A. Capria, "High range resolution multichannel DVB-T passive radar," *IEEE Aerosp. Electron. Syst. Mag.*, vol. 27, no. 10, pp. 37–42, Oct. 2012.

[15] J. L. Barcena-Humanes, J. Martin-de-Nicolas, C. Solis-Carpintero, M. P. Jarabo-Amores, M. Rosa-Zurera, and D. Mata-Moya, "DVB-T ambiguity peaks reduction in passive radar applications based on signal reconstruction," in *Proc. 11th Eur. Radar Conf.*, Oct. 2014, pp. 1900–1903.

[16] M.-P. Jarabo-Amores *et al.*, "IDEPAR: A multichannel digital video broadcasting-terrestrial passive radar technological demonstrator in terrestrial radar scenarios," *IET Radar, Sonar Navigat.*, vol. 11, no. 1, pp. 133–141, Jan. 2017.

[17] D. Olivadese, E. Giusti, D. Petri, M. Martorella, A. Capria, and F. Berizzi, "Passive ISAR with DVB-T signals," *IEEE Trans. Geosci. Remote Sens.*, vol. 51, no. 8, pp. 4508–4517, Aug. 2013.

[18] M. Martorella, E. Giusti, F. Berizzi, A. Bacci, and E. D. Mese, "ISAR based techniques for refocusing non-cooperative targets in SAR images," *IET Radar, Sonar Navigat.*, vol. 6, no. 5, pp. 332–340, Jun. 2012.

[19] D. Gromek, P. Samczynski, K. Kulpa, and M. K. Baczyk, "A concept of using MapDrift autofocus for passive ISAR imaging," in *Proc. Int. Conf. Radar Syst. (Radar)*, Oct. 2017, pp. 1–6.

[20] A. Manno-Kovacs, E. Giusti, F. Berizzi, and L. Kovacs, "Image based robust target classification for passive ISAR," *IEEE Sensors J.*, vol. 19, no. 1, pp. 268–276, Jan. 2019.

[21] K. E. Olsen and K. Woodbridge, "Analysis of the performance of a multiband passive bistatic radar processing scheme," in *Proc. Int. Waveform Diversity Design Conf.*, Aug. 2010, pp. 142–149.

[22] K. E. Olsen and K. Woodbridge, "Multiband passive bistatic DVB-T radar range resolution improvements and implications," in *Proc. 13th Int. Radar Symp.*, May 2012, pp. 28–31.

[23] K. E. Olsen and K. Woodbridge, "Performance of a multiband passive bistatic radar processing scheme—Part I," *IEEE Aerosp. Electron. Syst. Mag.*, vol. 27, no. 10, pp. 16–25, Oct. 2012.

[24] K. E. Olsen and K. Woodbridge, "Performance of a multiband passive bistatic radar processing scheme—Part II," *IEEE Aerosp. Electron. Syst. Mag.*, vol. 27, no. 11, pp. 4–14, Nov. 2012.

[25] D. Wehner, *High-Resolution Radar*. 2nd ed. Norwood, MA, USA: Artech House, Dec. 1994.

[26] K. E. Olsen, K. Woodbridge, and I. A. Andersen, "FM based passive bistatic radar target range improvement—Part II," in *Proc. 11-th Int. Radar Symp.*, 2010, pp. 1–8.

[27] C. Moscardini, M. Conti, F. Berizzi, M. Martorella, and A. Capria, "Spatial adaptive processing for passive bistatic radar," in *Proc. IEEE Radar Conf.*, May 2014, pp. 1061–1066.

[28] G. Bournaka, J. Heckenbach, A. Baruzzi, D. Cristallini, and H. Kuschel, "A two stage beamforming approach for low complexity CFAR detection and localization for passive radar," in *Proc. IEEE Radar Conf. (RadarConf)*, May 2016, pp. 1–4.

[29] N. del Rey-Maestre, D. Mata-Moya, M.-P. Jarabo-Amores, P.-J. Gómez-del Hoyo, J.-L. BÃĺrcena-Humanes, and J. Rosado-Sanz, "Passive radar array processing with non-uniform linear arrays for ground target's detection and localization," *Remote Sens.*, vol. 9, no. 7, pp. 1–29, 2017. [Online]. Available: http://www.mdpi.com/2072-4292/9/7/756

[30] J. J. van de Beek, M. Sandell, and P. O. Borjesson, "ML estimation of time and frequency offset in OFDM systems," *IEEE Trans. Signal Process.*, vol. 45, no. 7, pp. 1800–1805, Jul. 1997.

[31] N. J. Willis, *Bistatic Radar*. Rijeka, Croatia: SciTech, 2005.

[32] The DVB-T Standard, "Digital Video Broadcasting (DVB): Frame structure, channel coding and modulation for digital terrestrial television (DVB-T)," Eur. Telecommun. Standards Inst., Sophia Antipolis, France, Tech. Rep. ETSI EN 300 744, 2004.

[33] N. del-Rey-Maestre, J.-L. Barcena-Humanes, J. Rosado-Sanz, P. Gomez-del-Hoyo, and D. Mata-Moya, "DVB-T based passive radar performance sensitivity with respect to channel availability," in *Proc. Eur. Radar Conf. (EURAD)*, Oct. 2017, pp. 183–186.

[34] *N-Channel Scalable Coherent Receiver Datasheet—Coherent Receiver*. Accessed: Jul. 12, 2020. [Online]. Available: https://coherent-receiver.com/wp-content/uploads/2016/10/CoherentReceiverDat%asheet.pdf

[35] *Ettus Usrp B200/B210 Bus Series Datasheet—Ettus Research a National Instruments Company*. Accessed: Jul. 12, 2020. [Online]. Available: https://www.ettus.com/wp-content/uploads/2019/01/b200-b210_spec_sheet.pdf

[36] *Ettus Usrp N200/N210 Networked Series Datasheet—Ettus Research a National Instruments Company*. Accessed: Jul. 12, 2020. [Online]. Available: https://www.ettus.com/wp-content/uploads/2019/01/07495_Ettus_N200-210_DS_Flyer_HR_1.pdf

[37] *Ettus Usrp X300 And X310 X Series Datasheet—Ettus Research a National Instruments Company*. Accessed: Jul. 12, 2020. [Online]. Available: https://www.ettus.com/wp-content/uploads/2019/01/X300_X310_Spec_Sheet.pdf

[38] *Twin A/D PROCESSOR, User Manual*, Televes Corporation. Accessed: Jul. 12, 2020. [Online]. Available: https://www.televes.com/uk/564901-twin-processor.html

[39] T. M. Schmidl and D. C. Cox, "Robust frequency and timing synchronization for OFDM," *IEEE Trans. Commun.*, vol. 45, no. 12, pp. 1613–1621, Dec. 1997.

[40] H. Minn, V. K. Bhargava, and K. B. Letaief, "A robust timing and frequency synchronization for OFDM systems," *IEEE Trans. Wireless Commun.*, vol. 24, no. 5, pp. 822–839, May 2003.

[41] A. I. Bo, G. E. Jian-hua, and W. Yong, "Symbol synchronization technique in COFDM systems," *IEEE Trans. Broadcast.*, vol. 50, no. 1, pp. 56–62, Mar. 2004.
[42] E. del Castillo-Sanchez, F. J. Lopez-Martinez, E. Martos-Naya, and J. T. Entrambasaguas, "Joint time, frequency and sampling clock synchronization for OFDM-based systems," in *Proc. IEEE Wireless Commun. Netw. Conf.*, Apr. 2009, pp. 1–6.
[43] R. Cardinali, F. Colone, C. Ferretti, and P. Lombardo, "Comparison of clutter and multipath cancellation techniques for passive radar," in *Proc. IEEE Radar Conf.*, Apr. 2007, pp. 469–474.

Pedro-José Gómez-del-Hoyo received the M.Eng. degree in telecommunication engineering from the University of Alcalá, Madrid, Spain, in 2014. He is currently pursuing the Ph.D. degree focused on improved of detection and tracking techniques in multistatic passive radar systems. Since 2014, he has been with the High Frequency Technology Group, Department of Signal Theory and Communications, University of Alcalá. He has published five journal articles included in the Journal Citation Report and 37 conference papers. His research interests include signal models, radar signal processing, radar systems analysis and design, multistatic radars, and tracking techniques. He has been a member of the research team of several projects with public and private funding, including two projects funded by the European agencies or the European Commission and three projects funded by the Spanish Ministry of Economy and Competitiveness.

María-Pilar Jarabo-Amores (Member, IEEE) received the M.Eng. degree in telecommunication engineering from the Polytechnic University of Madrid, Spain, in 1997, and the Ph.D. (Hons.) degree in telecommunication engineering from the University of Alcalá, Madrid, Spain, in 2005.

Since 1997, she has been with the Signal Theory and Communications Department, University of Alcalá. She was an Assistant Professor from 1997 to 2003, a Lecturer from 2003 to 2008, an Associate Professor from 2008 to 2019, and a Full Professor since then. Her research interests include statistical signal processing, artificial intelligence systems, signal models, radar signal processing, and radar systems analysis and design. Her Ph.D. thesis dealt with the design of neural network-based radar detectors and was awarded with the Best Thesis Award in telecommunication engineering from the University of Alcalá. She is the author of more than 30 articles in international journals indexed in JCR, some book chapters and articles published by invitation in technical journals and more than 100 international conference papers. She has been involved in the research team of 25 international and national projects, in some of them as PI. She has supervised five Ph.D. thesis, two of them awarded by the Professional Telecommunication Association of Spain and the University of Alcalá.

David Mata-Moya (Member, IEEE) received the M.Eng. degree in telecommunication engineering and the Ph.D. (Hons.) degree in electrical engineering from the University of Alcalá, Madrid, Spain, in 2003 and 2012, respectively. Since 2004, he has been with the High Frequency Technology Group, Department of Signal Theory and Communications, University of Alcalá. His research interests include statistical signal processing, artificial intelligence systems, signal models, radar signal processing, and radar systems analysis and design. In these fields, he has published ten journal articles included in the Journal Citation Report and around 80 conference papers. He has been a member of the research team of several projects with public and private funding, including five projects funded by the European agencies or the European Commission, five projects funded by the Spanish Ministry of Economy and Competitiveness and seven projects with ICT companies as PI. He has supervised one Ph.D. thesis.

Nerea del-Rey-Maestre (Member, IEEE) received the M.Eng. degree in telecommunication engineering and the Ph.D. (Hons.) degree in telecommunication engineering from the University of Alcalá, Madrid, Spain, in 2012 and 2018, respectively. She is currently pursuing the Ph.D. degree focused on the design and optimization of robust detection techniques in presence of spatial and temporal variable clutter in passive radar scenarios. Since 2011, she has been with the High Frequency Technology Group, Signal Theory and Communications Department, University of Alcalá. She has published seven journal article included in the Journal Citation Report and 44 conference papers. Her research interests include radar signal processing, design and validation of radar detectors, statistical signal processing, and artificial intelligence systems. She has been a member of the research team of several projects with public and private funding, including three projects funded by the European agencies or the European Commission and three projects funded by the Spanish Ministry of Economy and Competitiveness.

Manuel Rosa-Zurera (Senior Member, IEEE) has been a Full Professor with the Signal Theory and Communications Department, University of Alcalá, since 2010. His main research interest includes statistical signal processing, with applications to detection and classification (speech, EEG, radar, and so on). In these fields is a coauthor of 63 articles in journal indexed in JCR, ten book chapters, and 178 papers presented in international conferences. He has supervised seven Ph.D. thesis, two of them awarded by the National Association of Telecommunication Engineers (ISDEFE Award to the best thesis in Defence) and five awarded as best thesis in telecommunication engineering from the University of Alcalá. He has been involved in 36 research projects with public funding, and 44 research contracts with companies. He has worked in three European projects (one as PI), and three projects funded by the European Defence Agency.

Dr. Rosa is an Associate Editor of IEEE ACCESS and *Electronics* (MDPI) journals and a reviewer of many international journals. He has been involved in the Technical Program Committee of several international conferences and has coordinated the Ph.D. Program in information and communication technologies from the University of Alcalá from 2004 to 2010. From 2004 to 2010, he was the Head of the Signal Theory and Communications Department and from 2010 to 2017, the Dean of the Polytechnic School of University of Alcalá. Since 2006, has been the Leader of the Applied Signal Processing Research Group. In 2008, this research team was awarded with the prize to Knowledge Transfer to Society and the Social Council of University of Alcalá.